Draft version April 13, 2015
Preprint typeset using LaTeX style emulateapj v. 12/16/11

DETECTING ACTIVE ASTEROIDS/COMETS FROM OSSOS SURVEY IMAGES

Authors
Affiliations
Draft version April 13, 2015

ABSTRACT

Abstract.
Keywords: keywords

1. INTRODUCTION

The active asteroids are small bodies in the main asteroid belt which have transient dust emission producing comet-like comae and tails. Unlike comets, which originate in the Kuiper Belt and Oort cloud, and have been scattered inwards by gravitational effects, the active asteroids have stable orbits confined to the main belt and likely formed in the same location as they reside presently (Sheppard and Trujillo 2015) (Fernandez et al. 2002). For objects which formed in the the outer region of the main belt, beyond the snow line, the crystallized water ice which was present at the time of formation and not exposed to primordial heating may still remain in reservoirs beneath the surface (Sonnett et al. 2011). According to models done by Fanale and Salvail (1989), beyond heliocentric distances of 2.4 AU ice can be protected against sublimation by a 'relatively thin' surface regolith of depth 1 – 100 m for the entire age of the solar system. If the ice layer were to be exposed to sub solar heating, sublimation could be triggered, ejecting dust particles from the surface producing a coma. The source of the dust emission may be different for each object and could include ice sublimation, impact ejecta, rotational instabilities due to YORP torques, or a combination of several effects. (Hsieh et al. 2015). As the source of the observed activity may not be a result of cometary ice sublimation, these objects are better known as active asteroids. Main belt comets are a subset of this group where ice sublimation is thought to be the source of the dust emission.

Since the first discovery of an active main-belt asteroid, 133P/Elst-Pizarro, several attempts have been made to identify new objects of this type; at present, eighteen objects have been identified (refer to Figure 1) (Jewitt et al. 2015). A comprehensive review of such searches can be found in Hsieh et al. (2015). A persistent challenge to this effort is that the detection of the coma or tails around small dark objects is highly dependent on the magnitude constraints of the survey. As most asteroids fall near the limiting magnitude of the survey in which they are discovered (Jewitt et al. 2015), objects which are larger, closer, or have higher albedo are preferentially detected and any dust emission would be more easily apparent. The active fraction of identified active asteroids greater than 1 km to main belt asteroids greater than 1 km is $f \sim 10^5$, and describes a strong lower limit as many objects are yet undetected. (Jewitt et al. 2015)

In this paper, we present a study using the Canada-France-Hawaii Telescope (CFHT) Outer Solar System Origins Survey (OSSOS) data to identify the presence of cometary activity in previously discovered asteroids. We select the Hungaria family as the test group for our search pipeline. Previously undetectable emission activity may be able to be identified from this data set, which was designed to detect trans neptunian objects, as the limiting magnitude (24.5 mag) is much lower than previous surveys Hsieh et al. (2015). The survey covers a wide field of both the ecliptic plane and low inclinations, and observes with long (> 287 s) exposures, allowing for the potential serendipitous discovery of active dust emission which was previously too faint to detect. In this study we intend to observe a number of asteroids in the OSSOS data set and identify potential activity by measuring the asteroidal point spread function (PSF) and comparing this to a computed stellar model PSF in order to detect a large deviation potentially characteristic of a coma or jet around the asteroid. Objects which indicate activity are then visually examined.

2. OBSERVATIONS

Observations taken by OSSOS with the CFHT MegaPrime wide-field optical imaging facility at the summit of Mauna Kea, Hawaii, have been collected since 2013. The wide-field imager, MegaCam, consists of a 36 CCD image plane, each 2048 x 4125 CCD with resolution of 0.185"/pix. This covers a field of roughly 1° x 1° on the sky. Each block of data taken consists of a mosaic of 21 segments of one-square-degree sky coverage, and at present, covers two orbital phase spaces on the plane of the ecliptic, and two off plane at low inclinations. MegaCam observes in the optical to near infrared with filters u*, g', r', i', and z'. Of these, r' and u* are the best suited filters for observing main belt objects, and the analysis presented only includes observations made using these filters. [todo: reword]

The OSSOS images are reduced ... [todo: how reduced]. (standard data detrending???) Source characteristic measurements were obtained from source extraction (SEP 2015) and were used to extract the orbital information the transient object.

3. ANALYSIS

From the calculated arcs provided by SSOIS (SSOIS 2015) of objects identified as asteroids in the AstDys catalogue (AstDys 2015) we were able to predict which asteroids were present in the OSSOS data set, and select these objects to be examined for cometary activity. From a set of 3528 images with exposure times greater than 200s, there are [todo: fill in] observations of [todo:

fill in] asteroids in the OSSOS data. We analyze a small group of objects in the Hungaria family as our test case for our automated pipeline. Of the 1187 Hungarias we have 76 observations of 25 objects.

3.1. *Object identification*

An automated pipeline was written to identify each asteroid in an OSSOS exposure by, in order of 'priority': it's location relative to the predicted coordinates, elongation due to trailing effects caused by the apparent rate of motion and the duration of the exposure, and apparent magnitude. The coordinates of each object in the exposure were obtained from photometric software (SEP 2015), and objects which were closest to the predicted location of the asteroid in question as calculated by JPL (2015) were chosen as candidate object. The expected elongation of the trail was calculated from the predicted motion of the asteroid over the length of the exposure (JPL 2015) under the assumption of constant motion. This value was then compared to the elliptical shape parameters calculated by the photometry of each candidate object. A difficulty in this process is that objects which are moving faster during the exposure, and thus trailed to a greater extent, will have their flux spread over a larger more oblong area and the photometry – which is optimized for point like sources and extended objects such as galaxies – inaccurately measures the shape of the object with an elliptical aperture. The underestimation of the length of the object will result in an inaccurate measurement of the elongation as well as the astrometry and photometry of the object. We therefore expect a correlation between elongation and the probability of flux measurement error, and we implement an error of 20 percent on measured elongation. The objects were also subject to a magnitude constraint, albeit with an large uncertainty for two reasons. The first is because objects which are active and have jets or a coma will appear brighter than the expected magnitude calculated from previous observations. Depending on the extent of the activity, this could cause the object to be measured as several magnitudes greater than predicted. For this reason we did not exclude objects which were bright than expected. And second, for the same reason as discussed with respect to the elongation uncertainty the accuracy of the magnitude measurements are correlated with the elongation of the trail. This is a result of the total flux of the object being spread over a larger area than the PSF which reduces the per unit area apparent magnitude and signal-to-noise (Veres et al. 2012). A direct consequence is a lowered limiting magnitude for fast moving asteroids. Additionally, the inaccurate measurement of the flux results in an uncertainty in the photometric flux weighted barycentre of the object. The centre coordinates was therefore chosen as the centre of the elliptical aperture for fast moving objects. For these reasons an uncertainty of 2 magnitudes was arbitrarily chosen, and as the information is not necessarily indicative of an accurate identification, an object which did not meet this condition was not rejected nor flagged. Alternatively, asteroids which were not the expected shape, but satisfied the coordinate and magnitude condition were flagged for human inspection. Cases of the asteroid being too close to bad pixels, the edge of the CCD, or involved with bright sources would be removed at this step of the pipeline. For exposures where the elongation ratio was greater than 1:5 [todo: check value, implement] the photometry measured the asteroid as two separate sources, and the image was flagged for human inspection. If more than one source met the same level of criteria but the object was not expected to be greatly elongated, the image was flagged separately for review.

In order to accurately measure the PSF of the asteroid, which is necessary to check for anomalous flux surrounding the object that could indicate activity, it is necessary to ensure that the asteroid is isolated from other sources. This was preformed with a comparison with a catalogue of bright sources built for the OSSOS images (OSSOS 2015) in the region surrounding the asteroid, and the cases where the asteroid was involved were discarded.

To ensure that every asteroid could be accounted for in the pipeline process, exposures where no source was found by the photometry in the region surrounding the predicted location of the asteroid, no objects met the elongation nor magnitude conditions, and images which failed to be processed by the photometry were also recorded to be reprocessed.

Applying this identification process left [fill in] objects to be examined.

3.2. *PSF comparison*

A postage stamp of size 2.5 times the full-width-half-maximum (FWHM) and centred on the midpoint of the elongated shape was rotated according to the angle of trailing, and a brightness profile was measured. Due to saturation effects, asteroids with magnitudes greater than 18.5 were not analyzed for activity. However, as previous surveys have included this set of objects Hsieh et al. (2015) we were comfortable with this exclusion. The PSFs were then compared to the stellar model PSFs built from the OSSOS MOP (OSSOS 2015) which were rotated by the same angle. A 3 sigma difference between the subtracted PSFs was used to indicate the presence of additional flux around an asteroid. There were [fill in] asteroids which were measured to be above this limit and were flagged for visual confirmation.

3.3. *Detection Efficiency*

4. DISCUSSION

As the involvement check was preformed using a catalogue of bright objects, it is possible that some asteroids identified and carried through the pipeline process were involved with dim background objects. An example of this is shown in figure 3. Depending on the geometry of the involvement this could be selected as an asteroid with activity, possibly a large bright jet. In order to distinguish between activity and involvement, the asteroids with unusual PSF's were all manually reviewed. Through this process we could determine whether a jet was present, in which case the outflowing dust would also have a trailing effect through the exposure, or if it were a case of involvement. We do not expect that a jet would be present for a fraction of the exposure time during one observation.

5. RECOMMENDATIONS

Use a trail fitting function for improved photometry on fast moving objects such as described by Veres et al. (2012).

Acknowledgments.

REFERENCES

AstDys, 2015. URL http://hamilton.dm.unipi.it/astdys/index.php?pc=5.

Fraser Fanale and James Salvail. The water regime of asteroid (1) ceres. *Icarus*, 82:97–100, 1989.

Julio A. Fernandez, Tabare Gallardo, and Adrian Brunini. Are there many inactive jupiter-family comets among the near-earth asteroid population? *Icarus*, 159:358?–368, 2002.

Henry Hsieh, L. Denneau, and R.J. Wainscoat. The main-belt comets: the pan-starrs1 perspective. *Icarus*, 2015.

David Jewitt, Henry Hsieh, and Jessica Agarwal. The active asteroids. *Asteroids IV*, 2015. arXiv:1502.02361v1 [astro-ph.EP].

JPL, 2015. URL http://hamilton.dm.unipi.it/astdys/index.php?pc=5.

OSSOS, 2015. URL http://www.cfht.hawaii.edu/en/science/LP_13_16/OSSOS.pdf. PI name Brett Gladman.

SEP, 2015. URL http://sep.readthedocs.org/en/v0.3.x/.

Scott Sheppard and Chadwick Trujillo. Discovery of the fast spinning main belt comet (62412) 2000 sy178. *The Astronomical Journa*, 149:44, 2015. arXiv:1410.1528 [astro-ph.EP].

S. Sonnett, J. Kleyna, and R. Jedicke. Limits on the size and orbit distribution of main belt comets. *Icarus*, 215:534–546, 2011. arXiv:1108.3095v1 [astro-ph.EP].

SSOIS, 2015. URL http://www4.cadc-ccda.hia-iha.nrc-cnrc.gc.ca/en/ssois/. This research used the facilities of the Canadian Astronomy Data Centre operated by the National Research Council of Canada with the support of the Canadian Space Agency.

The International Astonomical Union, 2015. URL http://www.minorplanetcenter.net/iau/MPCORB.html.

Peter Veres, Robert Jedicke, Larry Denneau, Richard Wainscoat, Matthew J. Holman, and Hsing-Wen Lin. Improved asteroid astrometry and photometry with trail fitting. *The Astronomical Society of the Pacific*, 124:1197–1207, 2012.

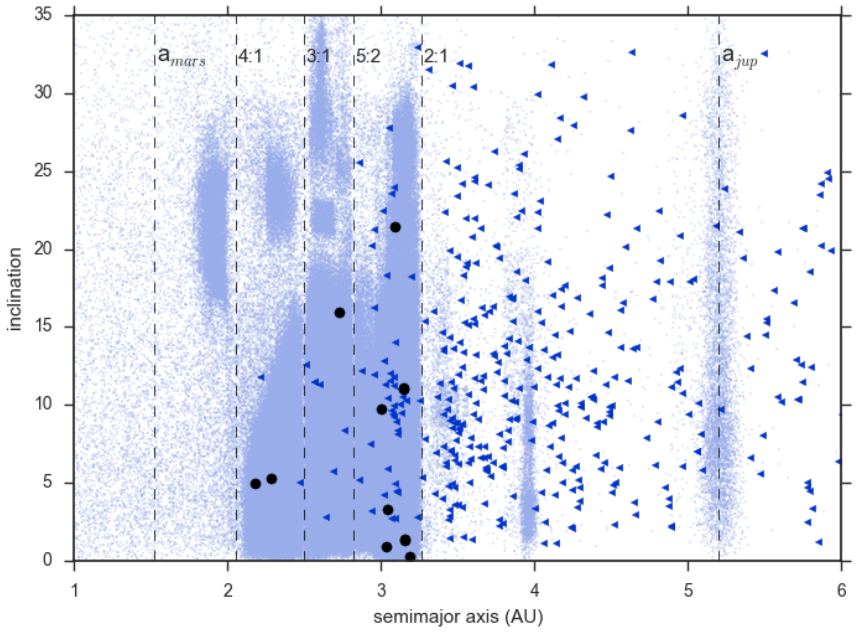

Figure 1. Inclination of all known objects in the main asteroid belt as a function of semimajor axis. Mean motion resonances between Mars and Jupiter as well as the planet's semimajor axis are marked in dashed lines, main belt objects are marked as light small dots, comets as arrows, and active asteroids as stars. Union (2015)

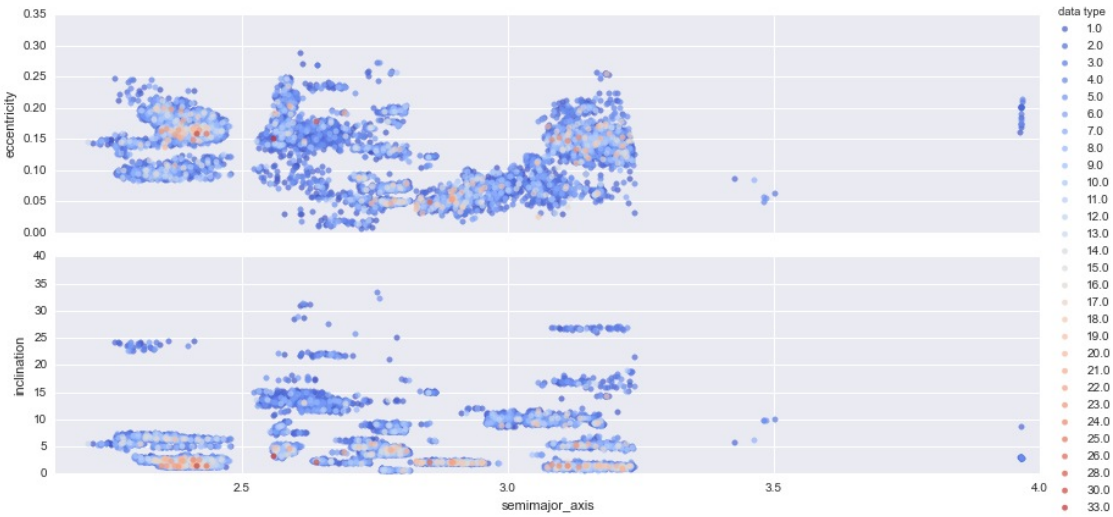

Figure 2. Inclination and eccentricity as a function of semi-major axis of all objects. Colours represents number of observations (occurrences) used in the analysis

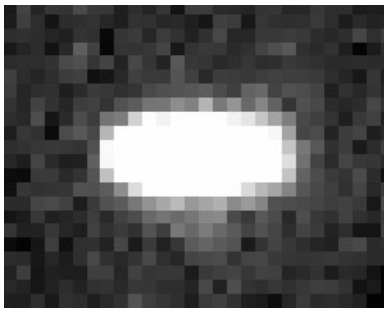

Figure 3. An asteroid involved with a dim background object.